APPLIED SCIENCES AND ENGINEERING

Adoptive T_{reg} therapy with metabolic intervention via perforated microneedles ameliorates psoriasis syndrome

Wentao Zhang[1]†, Yingxin Chen[1,2]†, Zhengjie Zhao[1], Hanqi Zheng[1], Shenqiang Wang[1], Ziyan Liao[1], Tao Sheng[1], Sheng Zhao[1], Wenhui Hou[1], Xinmin Yu[1], Fang He[3], Jicheng Yu[1,4,5,6,7], Yuqi Zhang[1,3,7]*, Zhen Gu[1,4,5,6,7,8]*

Regulatory T (T_{reg}) cells underlie multiple autoimmune disorders and potentialize an anti-inflammation treatment with adoptive cell therapy. However, systemic delivery of cellular therapeutics often lacks tissue targeting and accumulation for localized autoimmune diseases. Besides, the instability and plasticity of T_{reg} cells also induce phenotype transition and functional loss, impeding clinical translation. Here, we developed a perforated microneedle (PMN) with favorable mechanical performance and a spacious encapsulation cavity to support cell survival, as well as tunable channels to facilitate cell migration for local T_{reg} therapy of psoriasis. In addition, the enzyme-degradable microneedle matrix could release fatty acid in the hyperinflammatory area of psoriasis, enhancing the T_{reg} suppressive functions via the fatty acid oxidation (FAO)–mediated metabolic intervention. T_{reg} cells administered through PMN substantially ameliorated psoriasis syndrome with the assistance of fatty acid–mediated metabolic intervention in a psoriasis mouse model. This tailorable PMN could offer a transformative platform for local cell therapy to treat a variety of diseases.

INTRODUCTION

Autoimmune diseases subvert immune homeostasis partially by disrupting the balance of autoreactive T cells and suppressive regulatory T (T_{reg}) cells (*1*). For example, T_{reg} cells have been implicated as numerical and functional defects in the pathogenesis of multiple autoimmune diseases including psoriasis, type 1 diabetes, rheumatoid arthritis, and multiple sclerosis (*2*, *3*). Targeting T_{reg} cells for immunotherapy has emerged as a focus for curing or controlling autoimmune diseases, which could take advantage of the functional adaptability of T_{reg} cells to inhibit the activation and proliferation of immune effector cells, thereby restoring immunological self-tolerance and homeostasis (*4*). However, the survival of adoptive cells is challenged by external damages throughout the cell delivery process (*5*, *6*). In addition, the intrinsic unstable nature of T_{reg} cells further hinders the translation of T_{reg} therapy: The instability and plasticity of T_{reg} cells readily induce T_{reg} phenotype transition, thus compromising the related suppressive functions (*1*). Therefore, T_{reg} therapy that maintains cell survival, as well as restores and amplifies T_{reg} suppressive functions could offer a promising strategy for the treatment of autoimmune diseases (*3*, *7*–*9*).

Here, we develop a perforated microneedle (PMN) featured with channels on the shell and T_{reg} cell–loaded gel inside to ensure the cell survival and function for adoptive cell therapy in psoriasis (Fig. 1A). The clinical investigations of T_{reg} therapy have witnessed incremental therapeutic potential in psoriasis, a localized autoimmune skin disorder (*9*–*11*), acting as an alternative method to address the limited remission rate and lifelong management associated with the conventional medications or photo-based therapies (*8*). However, systemically administered T_{reg} cells usually have limited accumulation in the pathological epidermis due to sparse expression of skin-homing receptors, which could also cause off-target effects on other organs (*12*, *13*). Conversely, local T_{reg} therapy encounters impediments in treating dermatological disorders, primarily the challenge of transdermal cell delivery due to the impermeable nature of the stratum corneum barrier. In this study, the hydrophobic shell of PMN endows a spacious cavity for cell encapsulation to avoid nutrient depletion and unfavorable environment, thereby extending the lifespan of loaded cells. The PMN also offers sufficient mechanical strength to pierce through the desquamated skin and effectively deliver therapeutic cells into the pathological lesion, where the encapsulated cells spontaneously migrate out of the PMN through the designed channels on the shell. Moreover, the polymeric microneedle (MN) matrix made of poly(vinyl propionate-*co*-methyl methacrylate) [poly(VP-*co*-MMA)], an enzyme-degradable material, could release propionate in the inflammatory environment to enhance T_{reg} suppressive functions via the fatty acid oxidation (FAO)–mediated metabolic intervention (*14*, *15*). The PMN-mediated adoptive T_{reg} therapy increased the local $Foxp3^+$ T_{reg} population and strengthened the anti-inflammation responses through decreasing leukocyte infiltration, suppressing inflammatory cytokines expression, and mediating the balance

[1]Key Laboratory for Advanced Drug Delivery Systems of Zhejiang Province, College of Pharmaceutical Sciences, Zhejiang University, Hangzhou 310058, China. [2]Institute of Advanced Magnetic Materials and International Research Center for EM Metamaterials, College of Materials and Environmental Engineering, Hangzhou Dianzi University, Hangzhou 310018, China. [3]Department of Burns and Wound Center, Second Affiliated Hospital, School of Medicine, Zhejiang University, Hangzhou 310009, China. [4]Department of General Surgery, Sir Run Run Shaw Hospital, School of Medicine, Zhejiang University, Hangzhou 310016, China. [5]Jinhua Institute of Zhejiang University, Jinhua 321299, China. [6]Liangzhu Laboratory, Zhejiang University Medical Center, Hangzhou 311121, China. [7]National Key Laboratory of Advanced Drug Delivery and Release Systems, Zhejiang University, Hangzhou 310058, China. [8]MOE Key Laboratory of Macromolecular Synthesis and Functionalization, Department of Polymer Science and Engineering, Zhejiang University, Hangzhou 310027, China.
*Corresponding author. Email: guzhen@zju.edu.cn (Z.G.); yqzhang21@zju.edu.cn (Y.Z.)
†These authors contributed equally to this work.

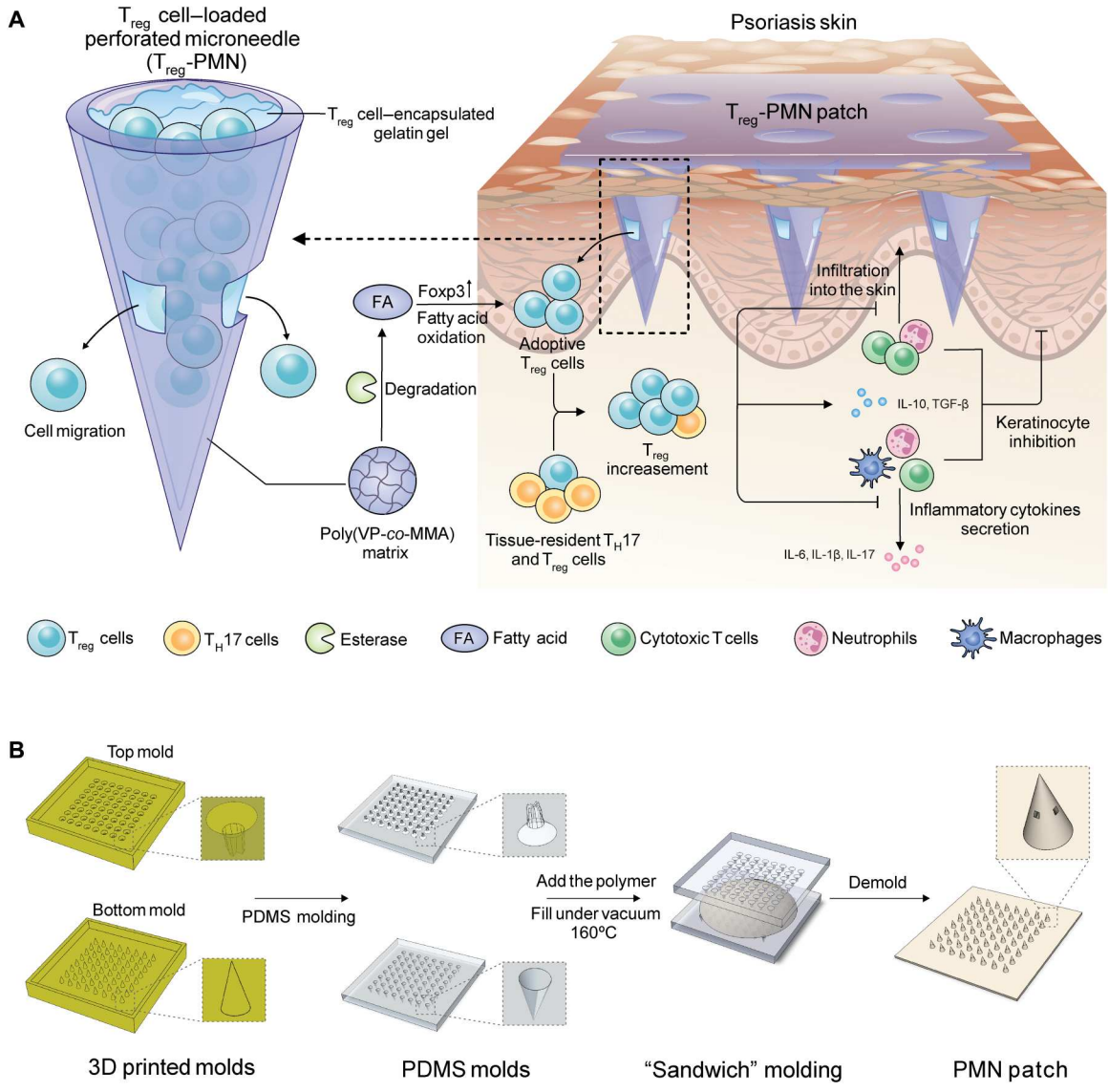

Fig. 1. Design of PMN-mediated adoptive T_{reg} therapy to alleviate psoriasis.. (**A**) Schematic illustration of the PMN patch in treating psoriasis: The loaded T_{reg} cells could migrate out of the PMN through designed channels into psoriasis skin and increase the number of suppressive T_{reg} cells; meanwhile, the PMN matrix [poly(VP-*co*-MMA)] could be degraded by esterase to generate fatty acid for enhanced expression of Foxp3 in T_{reg} cells, thereby strengthening the suppressive immunotherapy to ameliorate psoriasis syndrome. (**B**) The manufacturing processes of PMN with 3D printed molds via a sandwich molding method. T_H17, T helper 17; IL-10, interleukin-10; PDMS, polydimethylsiloxane.

of immune homeostasis. In vivo results demonstrated that T_{reg}-loaded PMN with fatty acid–releasing properties substantially mitigated the psoriasis syndrome in an imiquimod-induced psoriasis mouse model. This PMN system could also serve as a broad platform for local delivery of therapeutic cells such as stem cells and chimeric antigen receptor (CAR)–T cells to potentiate treatment efficacy and alleviate systemic side effects.

RESULTS

Design and characterization of the PMN

Noticeable advances in biomaterials have been witnessed in manipulating cell fates, modulating immune responses, and troubleshooting off-target side effects through tunable properties and controlled delivery by injectable hydrogel, implantable scaffold, and MN (*16*, *17*). In terms of MN, porous MN, cryo-MN, and core-shell MN have been explored for transdermal administration of adoptive cells, taking advantage of their preeminent penetration ability (*5*, *6*, *18*). However, porous MNs are usually limited by inadequate cell-residing capacity (*19*), whereas core-shell MN may hinder the release of inner cells due to the slow degradation of the hydrophobic shell, accounting for the inevitable cell death (*20*). To this end, we designed core-shell–structured PMN featured with tunable channels on the shell, granting desired mechanical properties, spacious loading cavity, and free cell migration for

transdermal delivery of therapeutic cells with sustainable viability and bioactivity.

To achieve the delicate MN designs, stereolithography three-dimensional (3D) printing technique, which exhibits high stability and resolution in microscale fabrication was used (*21*). However, the materials of 3D printer-generating MN often limit to photocurative resin, which can be toxic to the living cells (fig. S1). To take advantage of the 3D printing resolution but overcome the material limitation, PMN was fabricated through a "sandwich" molding method via squeezing two polydimethylsiloxane (PDMS) molds together with biocompatible polymer in between to generate the perforated MN (Fig. 1B). We assessed four different 3D designs for the feasibility and reproducibility in micromolding processes (fig. S2), wherein the design II exhibited desirable properties in 3D printer resolution and demolding process (fig. S3). The resulting PMN has four rectangular channels on the shell (length:145.9 ± 10.1 μm, width: 82.6 ± 4.6 μm), and the needles are designed as 300 μm in radius, 1100 μm in height, and 1400 μm in center-to-center distance (Fig. 2A). The hollow structure of PMN was evidenced by the section views at different layers, suggesting the regular shell structure and a spacious cavity (calculated as 0.148 μl per MN) (Fig. 2, B and C). This sandwich molding technique could be applied to multiple polymerized materials that conventionally can hardly yield a well-defined 3D structure, including poly(lactic-*co*-glycolic acid), polylactic acid, poly(methyl methacrylate) (PMMA), and polystyrene (fig. S4).

To support the hydrophilic culture medium, which helps maintain cell viability, an immiscible hydrophobic shell was preferred for PMN to avoid structural defects during administration. In addition to providing a favorable culture environment, it remains challenging to sustain the suppressive functionality of T_{reg} cells given its instability and plasticity. Recently, a preference for FAO over glycolysis at activating state in T_{reg} cells was characterized (*22*, *23*). Therefore, manipulating fatty acid availability could be a potential approach to implementing T_{reg} metabolic programming for treatments of autoimmune diseases or cancers (*22*, *24*, *25*). Therefore, we synthesized a hydrophobic copolymer [poly(VP-*co*-MMA)] of VP and MMA as the PMN matrix via bulk polymerization, which could not only tolerate the aqueous cell medium but also release propionate during the degradation by esterase enzyme, further enhancing T_{reg} function (fig. S5). The ratio of the monomers was adjusted to balance the mechanical properties and the amount of enzyme-degradable moieties of the MN (table S1). The addition of MMA could increase the stiffness of PMN up to 1.04 (±0.06) N per needle, while a higher percentage of VP tended to soften the structure (table S2). The ratio of the monomers

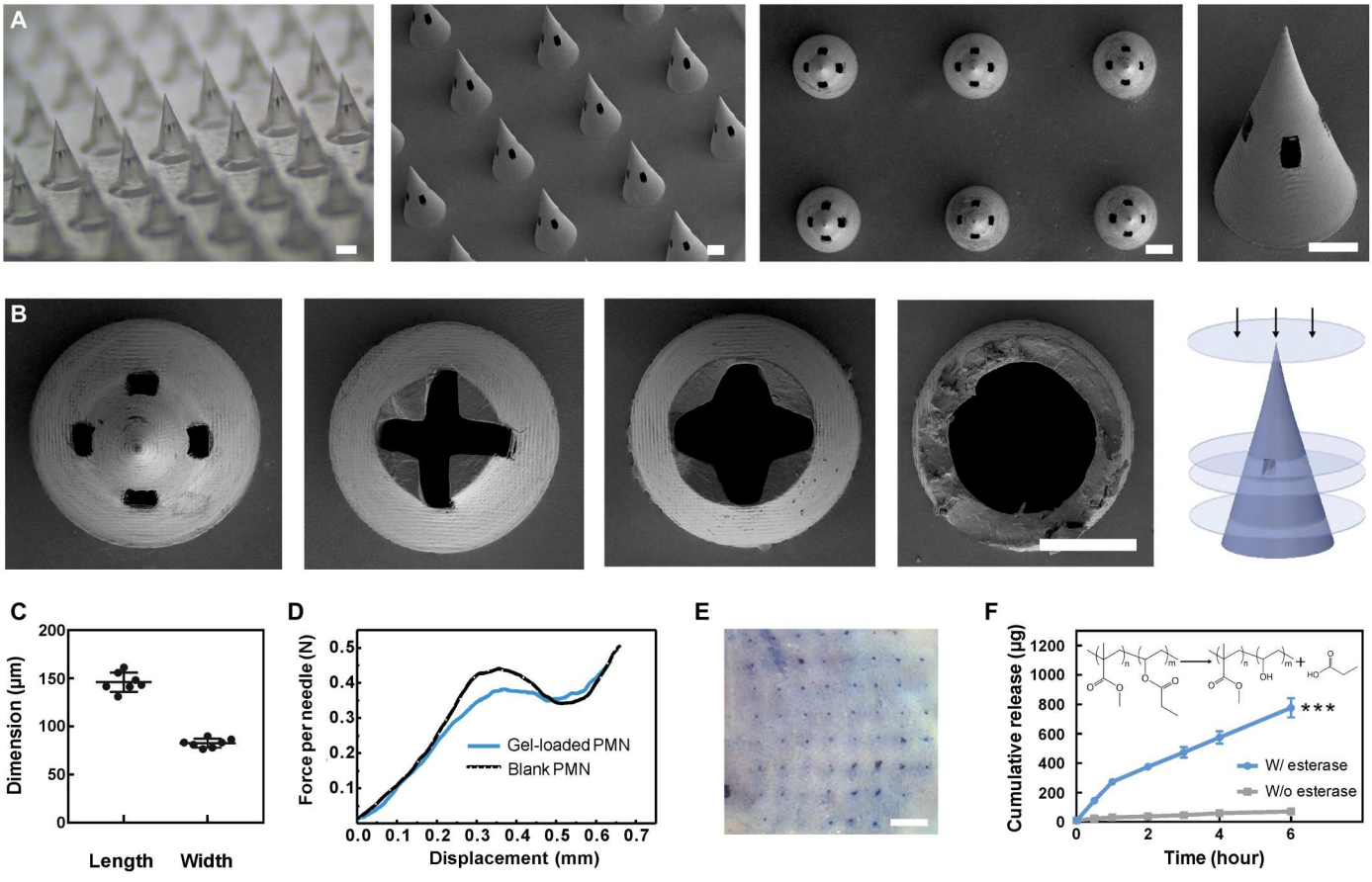

Fig. 2. The fabrication and characterization of PMNs. (**A**) Representative photograph and scanning electron microscopy (SEM) images of the PMNs. Scale bars, 300 μm, 200 μm, 300 μm, 200 μm (left to right). (**B**) SEM images displaying the cross-section of PMN at different layers. Scale bar, 300 μm. (**C**) Dimensions of channels on the PMN shell. $n = 7$. (**D**) Mechanical properties of the blank PMN and gel-loaded PMN. (**E**) Trypan blue staining image of mouse dorsal skin after administration of the PMN patch. Scale bar, 2 mm. (**F**) In vitro accumulated release of fatty acid from PMN in esterase (100 IU/ml). $n = 5$. ***$P < 0.001$. Data are means ± SD.

also influenced the glass transition temperature and therefore the manufacturing feasibility (fig. S6). Last, the volume ratio of VP to MMA in the copolymer poly(VP-*co*-MMA) was determined as 7:3 for the fabrication of PMN, the core-shell structure of which retained a strong penetration ability even with the hydrogel loaded inside (0.376 N per needle), also evidenced by the trypan blue staining image of PMN patch–pierced mouse skin (Fig. 2, D and E). Noteworthy, the cell toxicity test suggested an insignificant influence on cell viability compared to a widely used 3D printing material, the commercialized resin, demonstrating desired biocompatibility of poly(VP-*co*-MMA) for further cell delivery (figs. S1 and S7). To investigate the release behavior of fatty acid from the copolymer, esterase enzyme (100 IU/ml) was selected for in vitro release study to simulate the inflammatory microenvironment in the murine skin infected with psoriasis (*14*, *15*, *26*). The release profile indicated that the PMN could achieve a gradual release of propionate in an enzyme-mediated manner while remaining stable in the enzyme-free medium (Fig. 2F) (*15*).

Loading and release of T_{reg} cells from PMN

For loading therapeutic cells in the PMN system, a suitable medium should be determined to ensure cell survival, thereby endowing a prolonged therapeutic time window. Thermo-reversible gelatin was selected as the cell loading matrix, which maintained the survival of T_{reg} cells for 48 hours (fig. S8). T_{reg} cells (3.6×10^5) in 2% gelatin–RPMI-1640 medium were loaded into the PMN array (8 × 8) through vacuum. The successful loading was visualized by the confocal images of carboxyfluorescein diacetate succinimidyl ester (CFSE)–labeled T_{reg} cells embedded in PMN (Fig. 3A). Moreover, the viability of loaded cells in 2% gelatin remained at a comparative level (~82%) to those in RPMI 1640 medium throughout the loading process (Fig. 3B and fig. S9).

Next, we explored the release behavior of T_{reg} cells from the PMN. The channels on the shell were designed to allow the prompt migration of cells out of the PMN upon insertion into the release medium as observed in the video (movie S1), wherein most of the cells released in 1.5 hours (Fig. 3C). The migration rate slowed down in the Purecol hydrogel, indicated by the time-lapse images of the same layer of one PMN (Fig. 3, D and E). Accordingly, the release kinetics in vivo was even slower given the compact structure of skin tissue (fig. S10). The channel structure was preserved during the application as observed by the scanning electron microscopy (SEM) image, suggesting a constant cell release ability (fig. S11). The T_{reg} cells could also reside in the dorsal skin for an extended period after the patch removal (fig. S12). Together, PMN had desired cell loading capacity and delivery efficiency both in vitro and in vivo.

Enhanced T_{reg} cell suppression by PMN-derived fatty acid

Although the current understanding of psoriasis etiology remains ambiguous, abnormal autoreactive T cell activities were described in cutaneous immune homeostasis. In detail, suppressive T_{reg} cells that express Foxp3, the master regulator, can be converted to interleukin-17 (IL-17) releasing T helper 17 (T_H17)–like T_{reg} cells due to plasticity and instability, therefore further exacerbating the psoriasis syndrome (*27*–*29*). Previous research suggested that an unstable expression of Foxp3 might dampen the suppressive activity of T_{reg} cells, particularly during in vitro culture and stimulation (*30*, *31*). The in vitro culture results corresponded with previous findings that the Foxp3 expression decreased to 43.84 (± 8.45) % on day 3 and 16.68 (± 4.32) % on day 7 despite that the cell number climbed to 1.03 (±0.12)–fold and 1.95 (±0.22)–fold, respectively (Fig. 3, F and G).

To stabilize T_{reg} suppressive functions, FAO was introduced to manipulate T cell metabolism (*23*). Previous studies suggested that increased lipid oxidation could stabilize Foxp3 expression and enhance T_{reg} suppressive functions by Foxp3 acylation and other yet-to-be-established mechanisms (*32*, *33*). To explore the influence of exogenous fatty acid on Foxp3 stability, T_{reg} cells were cocultured with sodium propionate in different mediums. It was demonstrated that, with a daily refreshing medium, the insignificant difference of Foxp3 expression in T_{reg} cells was observed in 3 days (fig. S13A). On the contrary, in the condition without medium refreshment, the limited nutrients supplemented with sodium propionate triggered an elevated Foxp3 expression from day 2 (Fig. 3H), and this elevation manifested even earlier when culturing in a sparse nutrient medium (fig. S13B). These results could be attributed to the competition between fatty acid and glucose in nutrient supply and their respective roles in suppressive functions and proliferation of cells (*23*, *24*, *34*). In addition to stabilizing Foxp3 expression, we further assessed the effect of fatty acid on T_{reg} suppressive function. The T_{reg} suppression assays indicated that 2 mM sodium propionate augmented the suppression ability of T_{reg} on conventional T (T_{con}) cells, especially at T_{con}:T_{reg} ratios of 4:1 and 8:1 (Fig. 3I). This effect was even more pronounced for sodium butyrate (fig. S14). Notably, coincubation tests indicated that T_{reg} cells relied more on fatty acid compared to T_{con}, wherein fatty acids hindered T_{con} proliferation but not T_{reg}, about two- to fourfold for sodium propionate and 6- to 10-fold for sodium butyrate depending on the concentrations (Fig. 3J and fig. S15).

Inspired by the above results, we further validated whether the fatty acid derived from PMN could achieve similar effects as sodium propionate. Consistently, an increase of Foxp3 expression from day 2 and an enhanced suppression ability for all T_{con}: T_{reg} ratios were observed (Fig. 3, K and L). Notably, the esterase-mediated gradual release could avoid the enriched fatty acid concentration that may impose osmotic stress on T_{reg} cells (fig. S16).

In vivo evaluation of therapeutic efficacy in a mouse psoriasis model

We next evaluated the therapeutic efficacy of T_{reg} cell–loaded PMN (T_{reg}-PMN) in an imiquimod-induced psoriasis mouse model (Fig. 4A). BALB/c male mice at age around 8 to 9 weeks were selected. The mice were randomly divided into seven groups (n = 5 to 6), with one group applied with Vaseline as a healthy control group (normal) and six groups induced with psoriasis by imiquimod. Then, the psoriasis-bearing mice were treated with different formulations to evaluate the treatment efficiency: One group was chosen as a negative control without treatment (untreated), and the other five treatment groups were administered with blank MN (B-PMN), systematic injection of T_{reg} (i.v. T_{reg}), intradermal injection of T_{reg} (i.d. T_{reg}), T_{reg}-loaded perforated MN made of PMMA (T_{reg}-MMN), and T_{reg}-loaded PMN made of poly(VP-*co*-MMA) (T_{reg}-PMN). Typical clinical manifestations of psoriasis involved well-demarcated, thickened, erythematous scaly plaques on the skin surface, generated from uncontrolled keratinocytes hyperproliferation and massive immune cell infiltration (*10*). With the treatment of 6 days, T_{reg}-PMN substantially ameliorated psoriasis syndrome in

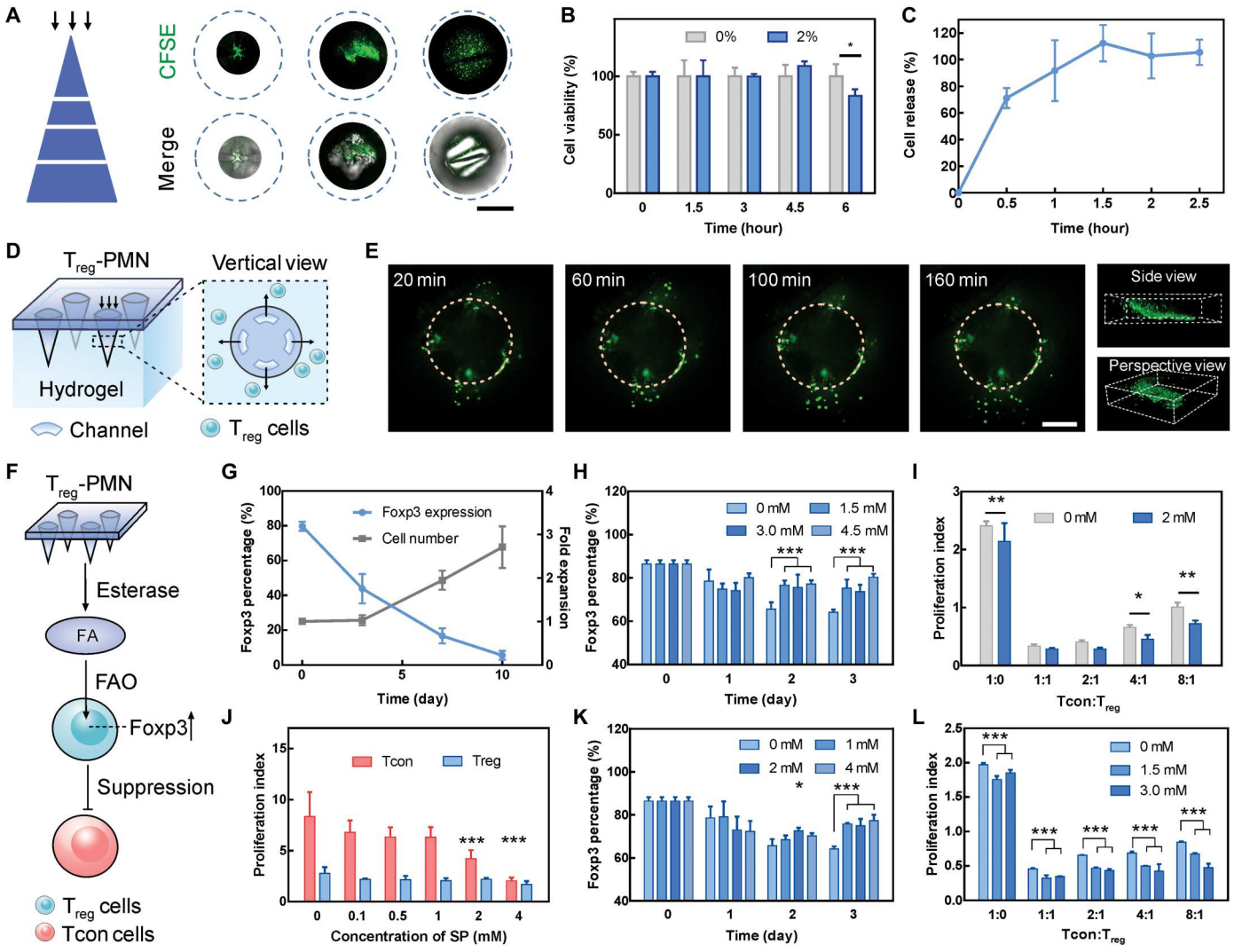

Fig. 3. The enhancement of T_{reg} functions by fatty acid derived from PMN. (**A**) Representative confocal images of the cross-section of T_{reg} cell–loaded PMN showing the CFSE-labeled T_{reg} cells. Scale bar, 200 μm. (**B**) T_{reg} cells viability throughout the loading process, as compared to the cells in 0% gelatin–RPMI 1640 medium at the same time point. $n = 4$. (**C**) In vitro accumulated release of T_{reg} cells from PMN into RPMI 1640 culture medium. $n = 4$. (**D**) Schematic showing the release of T_{reg} cells from PMN to the Purecol hydrogel. (**E**) Representative time-lapse images of PMN loaded with CFSE-labeled T_{reg} cells in the hydrogel and the 3D construct 2 hours after PMN administration. Scale bar, 200 μm. (**F**) Schematic of the in vitro enhancement of Foxp3 expression and suppressive ability of T_{reg} cells to T_{con} cells by PMN-derived fatty acid. FAO, fatty acid oxidation. (**G**) Foxp3 percentage and fold expansion of T_{reg} cells along with culture time extension. $n = 4$. (**H**) Foxp3 percentage in total T_{reg} cell population when culturing in a medium without refreshment. (**I**) T_{reg} suppression assay with or without sodium propionate (2 mM) supplement. (**J**) Proliferation index of T_{con} and T_{reg} when cocultured with different concentrations of sodium propionate. SP, sodium propionate. $n = 4$. (**K**) Foxp3 percentage in total T_{reg} cells population when culturing in a medium with PMN-derived fatty acid. (**L**) T_{reg} suppression assay with or without PMN-derived fatty acid. The proliferation index is calculated by the number of proliferated cells to the unproliferated cells. $n = 5$ for (**H**), (**I**), (**K**), and (**L**). All comparisons were made with 0 mM fatty acid. $^*P < 0.05$, $^{**}P < 0.01$, and $^{***}P < 0.001$. Data are means ± SD.

mice compared to those without treatments who experienced severe inflammation and keratinocytes hyperplasia (Fig. 4B). The Psoriasis Area and Severity Index (PASI) and heatmap were also consistent with the symptom observed from the images that the overall performance of T_{reg} cells administered via PMN was superior to other groups (Fig. 4, C and D, and fig. S17).

Specifically, the blank PMN exhibited inconspicuous curative effects compared to the untreated group, indicating that PMN-derived fatty acids alone could hardly reverse the disease. Although other treatment groups (i.v. T_{reg}, i.d. T_{reg}, and T_{reg}-MMN) except for T_{reg}-PMN also exhibited a deceleration in psoriasis progression and resisted the daily imiquimod induction, none of them performed equivalent effects compared to the group administered with T_{reg}-PMN. The systematically administered T_{reg} cells performed the least satisfied mitigation among the treatment groups even with a higher dosage (4×10^7 cells/kg) than the clinical-related standard (1×10^7 to 3×10^7 cells/kg) (*35*, *36*). Intradermal injection of T_{reg} cells exhibited competitive therapeutics efficacy in relieving epidermis thickness (induration) but not in erythema and desquamation, probably due to restricted cell migration and confined effective area compared to those treated with T_{reg}-PMN and T_{reg}-MMN. Compared to the systematic and the intradermal

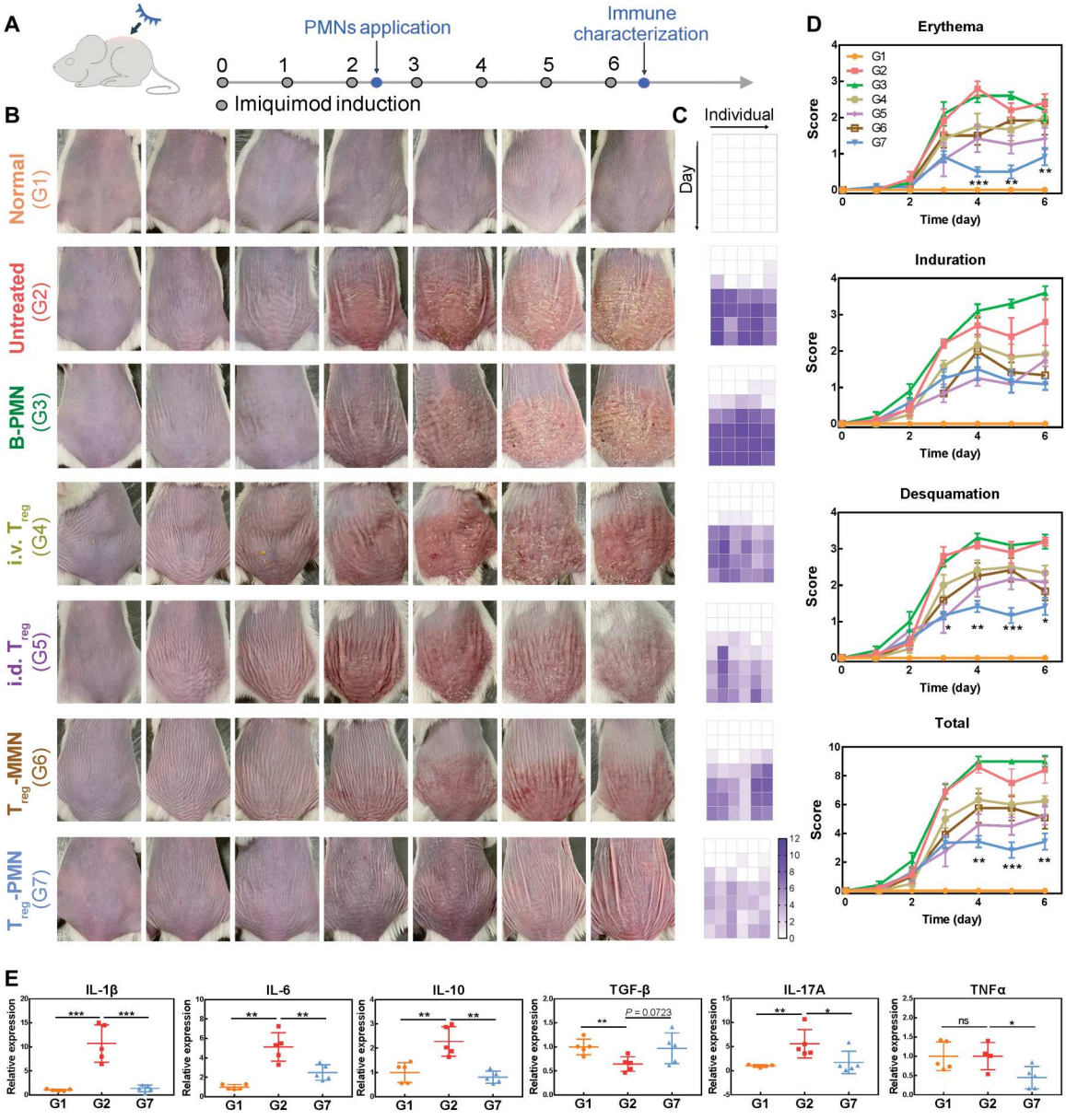

Fig. 4. Psoriasis alleviation by T_{reg}-PMN. (**A**) Schematic illustration of PMN-mediated psoriasis treatment. (**B**) Representative images of mice dorsal skins in different groups from days 0 to 6. $n = 4$ for the normal group, $n = 5$ for the untreated group and B-PMN, and $n = 6$ for the others. (**C**) Heatmap of PASI score (total) of each individual. (**D**) PASI score (erythema, induration, desquamation, and total) measured from days 0 to 6. Comparisons were made between T_{reg}-PMN (G7) and *i.v.* T_{reg} (G4) each day. (**E**) mRNA expression in mice dorsal skin measured by qRT-PCR 8 hours after PMN administration. $^*P < 0.05$, $^{**}P < 0.01$, and $^{***}P < 0.001$. Data are means ± SD. ns, not significant. TGF-β, transforming growth factor–β. TNFα, tumor necrosis factor–α.

injection, T_{reg} cells administered via PMN presented significant alleviation in erythema at days 4 and 5, improved in desquamation and total indexes at days 4 and 5, and equal in induration index from day 3.

To distinguish the effects of fatty acid in ameliorating psoriasis syndrome, T_{reg} cells were encapsulated in MMN made of PMMA, which was deprived of the ability to release fatty acids. Mice treated with T_{reg}-PMN revealed more considerable suppressive effects compared to those with MMN, especially in erythema index from days 3 to 5, but not in induration and desquamation. The differences could also be perceived by images from three representative individuals in both groups (fig. S18).

The possibility of psoriasis relapse was further excluded by monitoring the long-term psoriasis induction in T_{reg}-PMN and untreated psoriasis groups. The T_{reg}-PMN group resisted the continuous imiquimod application and remained in a less-severe skin condition, while the untreated psoriasis group slowly returned to the normal stage at around day 12 (fig. S19). These findings were consistent with previous report of self-recovery in the imiquimod-induced psoriasis mice model (*37*).

To further investigate the immunomodulatory effects of T_{reg}-PMN, we characterized the evolution of the immunological environment before and after the MN application. The adoptive transfer of T_{reg} cells was verified by fluorescence-activated cell sorting (FACS) analysis of mice dorsal skin 8 hours after PMN administration, wherein the $CD4^+Foxp3^+$ T_{reg} percentages increased from 5.44 to 30.2% (fig. S20). The mRNA expression levels of several cytokines were also measured by quantitative reverse transcription polymerase chain reaction (qRT-PCR) (Fig. 4E). Significantly elevated expressions during psoriasis deterioration and noticeable declines after the T_{reg}-PMN treatment were observed in IL-1β, IL-6, and IL-17A. The IL-10, conventionally perceived as anti-inflammatory and a major tool for T_{reg} suppression, was highly increased in psoriasis progression but declined after the treatment. This phenomenon was also observed in patients, and we attributed this to the pro-inflammatory aspect of IL-10, especially a role in $CD8^+$ functions and maintenance (*38*–*40*). The suppressive transforming growth factor–β (TGF-β) was significantly lower in the psoriasis group but recovered after the treatment ($P = 0.0723$). Slight differences were detected in IL-23R and IL-12b expression, probably due to the disease stage and negligible expression in the skin (fig. S21) (*41*, *42*).

The therapeutic efficacy was further evaluated on day 6, when all mice were euthanized for analysis of immune population and cytokines concentration. A holistic recovery from intense inflammation to a chronic stage was achieved via the treatment of T_{reg}-PMN as indicated by FACS and enzyme-linked immunosorbent assay (ELISA). It was found that a remarkable decrease of $CD45^+$ cells in the skin lesion administered with T_{reg}-PMN (2.81%) compared with the untreated group (6.44%) or the B-PMN group (5.08%) (Fig. 5A). There were also mild decreases in mice treated with T_{reg} cells intradermally and systematically, measured as 5.58 and 4.04%, respectively. In contrast to untreated psoriasis, T_{reg}-PMN was marked as fewer neutrophil infiltration and higher percentage of $Foxp3^+$ T_{reg} (Fig. 5B and fig. S22).

The amelioration effects of T_{reg}-PMN were also examined in the cytokine milieu (Fig. 5C). The higher levels of IL-10 and TGF-β1 and a lower IL-6 level were observed in the T_{reg}-PMN group, which were consistent with the higher percentage of $Foxp3^+$ T_{reg} cells and better overall performance (*10*). The moderate level of tumor necrosis factor–α in all treated groups indicated chronic psoriasis pathology (*43*). The concentrations of several psoriasis-associated cytokines (interferon-γ, IL-17A, IL-22, and IL-23) were statistically insignificant among the normal, untreated psoriasis, and T_{reg}-PMN groups, probably due to their overexpression in the exacerbating middle stage but not the recovering late stage of the psoriasis model (Fig. 5C and fig. S23) (*37*, *44*). The amelioration of keratinocyte hyperproliferation via T_{reg}-PMN could also be revealed by representative hematoxylin and eosin (H&E)–stained images. The dorsal skins from the untreated psoriasis and blank PMN groups experienced keratinocytes hyperplasia from 20.58 (±3.57) μm to 118.10 (±25.27) μm, but those of T_{reg}-PMN group only exacerbated to 66.24 (±9.72) μm (Fig. 5D). Despite other treatments alleviated the epidermal thickening, the mitigation effects of T_{reg}-PMN on hyperplasia was significantly distinguished, measured as 83.35 (±10.90) μm for i.d. T_{reg}, 83.13 (±12.39) μm for i.v. T_{reg}, and 88.29 (±15.11) μm for T_{reg}-MMN. Furthermore, we observed that the PMN-mediated Treg therapy exhibited reinforced mitigation effects on the local lesion rather than systemic syndrome (fig. S24).

DISCUSSION

Psoriasis affects more than 100 million individuals worldwide with negative impacts on quality of life and serious comorbidities in metabolism, arthritis, and cardiovascular system (*10*, *11*). Conventional treatments for autoimmune diseases such as psoriasis have longstanding clinical applications, but their effects remained erratic due to complicated disease triggers (*4*, *8*, *11*). The nonspecific immune-modulatory drugs are often accompanied by systematic side effects, mortalities, and low response rates (*4*). Upon the disclosure of T_{reg} suppressive roles in autoimmune diseases, T_{reg} therapy holds unprecedented promises in their managements by restoring immune self-tolerance (*1*, *7*). An adequate administration route that enables efficient T_{reg} cell delivery and an enriched population with retained survival and functions could expand the therapeutic potentials of T_{reg} therapy. MN provides feasible transdermal administration for the delivery of small molecules, peptides, genes, and proteins (*13*, *45*). However, limited investigations of MN-mediated cell delivery have been reported, given the volatile feature of living cells. In our study, the dedicatedly designed PMN fulfilled reinforced T_{reg} therapy for psoriasis by preserving cell viability, meanwhile promoting suppressive ability through fatty acid–mediated metabolic manipulation. In the psoriasis mouse model, the spacious cavity and sufficient penetration ability provided by PMN rendered feasibility for transdermal cell delivery. The tunable channels enabled desired cell release to achieve optimal therapeutic effects. Moreover, adoptive T_{reg} therapy mediated via PMN managed to strengthen anti-inflammation responses through decreasing leukocyte infiltration, especially the neutrophils; suppressing the secretion of inflammatory cytokines and enhancing the expression of anti-inflammatory cytokines; mediating the immune homeostasis and converting the disease to a mild state.

In addition, the sandwich molding fabrication offered extended selectivity of MN materials and tailored structure in terms of varied applications, such as combining the penetration ability of MN with the CAR-T cell immunotherapy in solid tumors or with stem cell therapy in regeneration medicine (*6*, *18*). Furthermore, PMN-assisted cell administration could also strengthen local therapeutic efficacy particularly for dermatological disorders, potentially reducing systematic side effects.

T cell metabolic programming holds promise to extend cell therapy by adjusting or maintaining the cell functions. Reported strategies such as fatty acid–releasing particles or direct fatty acid supplements to restore the mucosal homeostasis highlighted the vital role of short-chain fatty acid in T_{reg} cells (*15*, *32*, *46*, *47*). Metabolism could also affect the survival of cancer cells (Warburg effect) and the persistence of cytotoxic T cells, suggesting the potential of metabolic treatment in cancer immunotherapy (*48*, *49*). In addition, other approaches to extending the T_{reg} cell therapy have been proposed, such as T cell receptor–engineered T_{reg} cells to specialized anti-inflammation effects and IL-2/rapamycin as the stabilizers to maintain Foxp3 expression (*3*, *7*, *16*, *50*). Methods of ex vivo expanding T_{reg} cells, gene-engineered T_{reg} cells or "off-the-shelf" T_{reg} cells are also under intensive research (*3*, *7*). A holistic stabilization of suppressive functions of T_{reg} cells through multiple interventions could be combined and expected in the future. In summary, this PMN system offers a general platform for cell therapy in the treatment of autoimmune diseases, cancer therapy, and tissue engineering (*3*, *16*, *51*, *52*).

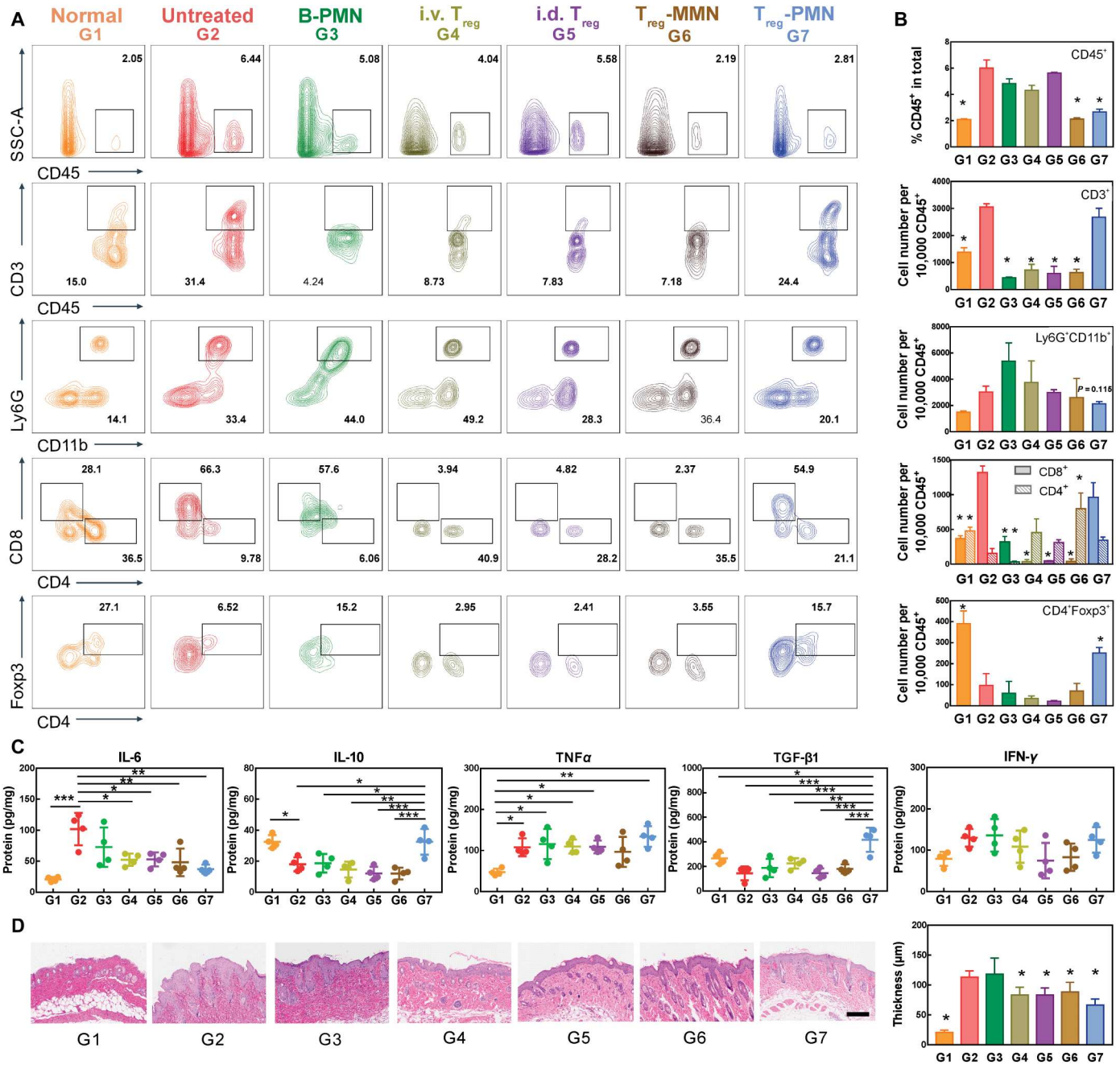

Fig. 5. The mitigation effects of T_{reg}-PMN to inflammatory environment in psoriasis. (**A**) Representative flow cytometry charts of $CD45^+$ cells, T cells ($CD3^+$), neutrophils ($Ly6G^+CD11b^+$), $CD8^+$ T cells, $CD4^+$ T cells, and $CD4^+Foxp3^+$ T_{reg} cells (all gated on $CD45^+$ or $CD45^+CD3^+$). (**B**) Quantification of leukocytes analyzed by flow cytometry. Comparisons are made with the untreated psoriasis group. $n = 2$; each sample represents a mixture of three independent mice. (**C**) Cytokine concentrations in the psoriasis lesion on day 6 as determined by ELISA. (**D**) Hematoxylin and eosin staining of the mice dorsal skin after different treatments on day 6 and corresponding epidermis thickness. Scale bar, 500 μm, $n = 9$. $^*P < 0.05$, $^{**}P < 0.01$, and $^{***}P < 0.001$. Data are means ± SD. SSC-A, side scatter area; IFN-γ, interferon-γ;

MATERIALS AND METHODS

Materials

All materials were purchased from Sinopharm Chemical Reagent Co. Ltd. unless specified elsewhere. 3D printing material, HTL, was purchased from BMF (Boston Micro Fabrication) Nano Materials Technology Co. Ltd. PDMS was purchased from Dow Inc. All cell culture reagents were purchased from Thermo Fisher Scientific. All primers (table S3) were synthesized by GenScript Biotech. All FACS antibodies were purchased from Univ-Bio. ELISA kits were purchased from MultiSciences Biotech Co. Ltd.

Synthesis of poly(VP-*co*-MMA)

VP and MMA were distilled to remove 4-methoxyphenol inhibitor and mixed in a volume ratio of 7:3 (VP:MMA) with 1% weight ratio

of azodiisobutyronitrile. The mixture (1 ml) was aspirated and sealed in a 3-ml vial and reacted for 48 hours at 60°C to obtain poly(VP-*co*-MMA).

Fabrication of PMN

The top and the bottom molds were 3D printed by BMF nanoArch S140 (BMF Nano Materials Technology Co. Ltd) with HTL resin and 10-μm resolution in *z*-axis. The MNs were placed in a 1.4-mm center-to-center spacing and arranged in an 8 × 8 array. The resulting molds were soaked in isopropanol overnight and dried in 90°C oven for 12 hours. Later, an ultraviolet (wavelength = 406 nm) light was projected to each facet of the two molds for at least 2 hours. Then, PDMS molds were obtained by demolding SYLGARD 184 Silicone from the treated molds. To obtain PMN, around 150 mg of poly(VP-*co*-MMA) was placed on the bottom PDMS mold in the vacuum oven at 160°C to remove excess air in the tip. The liquified material should be flat within 20 min and allowed to cool down at the ambient condition to form MN. The top PDMS mold was placed on the MN patch to make a sandwich. The sandwich later returned to 160°C oven, and the extrusion part of the top mold will slowly sink into the MN via gravity and gentle pressing. Last, PMN was obtained after cooling down to room temperature by peeling off the top mold.

Mechanical strength test

The mechanical strength of MN was tested by a compression testing machine (ZQ-990B, Zhiqu Precision Instrument, China) with descending force through a cylindrical tip with ≍10 mm in diameter. The moving speed of the cylindrical tip was set to 0.1 mm min^{-1}, and the recording threshold is >0.025 N.

Analysis of propionate released from poly(VP-*co*-MMA)

Poly(VP-*co*-MMA) was immersed into esterase PBS solution (100 IU/ml) at 158 mg/ml. The reaction was performed at 37°C for different time periods. At each time point, all medium was removed for analysis and replaced with the same amount of esterase solution. The release amount of propionate was determined by liquid chromatography with tandem mass spectrometry as the literature described (*53*).

T cell culture and suppression assay

T cells were isolated from the spleen by EasySep Mouse $CD4^+CD25^+$ Regulatory T Cell Isolation Kit II and Mouse T Cell Isolation Kit (STEMCELL Technologies) as the manufacturer instructed. For regular culture, all cells were cultured in the complete T cells culture medium (RPMI 1640 with 10% heat-inactivated FBS, 1× penicillin/streptomycin, 1× sodium pyruvate, 1× nonessential amino acids, 20 mM Hepes, and 50 μM β-mercaptoethanol) with IL-2 (30 IU/ml; PeproTech, catalog no. 200-02) for $CD3^+T_{con}$ and IL-2 (1500 IU/ml) for T_{reg} cells. The T Cell Activation/Expansion Kit (Miltenyi Biotec) was administrated at a cell-to-bead ratio of 3:1. Cell viability was determined by calcein AM and propidium iodide (PI) (Beyotime Biotech.). Cell number was counted by hemocytometer. For the T_{reg} suppression assay, T_{con} was dyed by CFSE and calculated as proliferation index (the number of proliferated cells to the unproliferated cells). For the sodium propionate suppression assay, different volumes of 50 mM sodium propionate were added to 10^5 T cell in 100-μl system to reach a final concentration of 1, 2, or 4 mM. For PMN-derived propionate suppression assay, PMN was immersed into esterase RPMI 1640 culture medium (100 IU/ml) at 158 mg/ml for 24 hours. Esterase was removed from the releasing medium by ultrafiltration. The propionate concentration was determined as previously described and supplemented with IL-2 and heat-inactivated fetal bovine serum. The Foxp3 expression was determined by FACS with anti-CD4 and anti-Foxp3 antibodies.

Cell loading

To obtain T_{reg}-loaded PMN, 2×10^7 T_{reg} cells were resuspended in 500 μl of T cell culture medium with 2% gelatin solution at 37°C, and then 100 μl of the Treg-gelatin medium was placed on the base of PMN patch in a vacuum oven for 2 min. The temperature 37°C should be constant, and water vapor should be saturated at the vacuum condition. The excessive medium can be recycled by piping off. Then, the T_{reg}-loaded PMN was stored at 4°C for 15 min to allow the gel formation before peeling off the bottom mold. For the animal experiments, T_{reg} cells were freshly isolated to avoid Foxp3 loss.

Cell release

Complete T cell culture medium was used as the releasing medium. For in vitro cell release, 200 μl of culture medium (1.7 ml in total) was extracted from the system at each time point, and the same amount of fresh medium was supplemented. The cell number in the extracted medium was calculated by a cell counter (Countess 3, Thermo Fisher Scientific) or hemocytometer five times to yield an average result. For release into 3D culture gel, 300 μl of Purecol–RPMI 1640 hydrogel was preseeded into the confocal dish and allowed for 4 hours to crosslink. T_{reg}-loaded PMN was pierced into the gel, and confocal images were taken at each time point without the MN removal. The in vivo live imaging was conducted by applying T_{reg}-loaded PMN to mice dorsal skin for different time periods (2, 4, or 6 hours), and the images were taken immediately after the patch removal. The long-term T_{reg} cell retention was observed by imaging the same mouse at different time points after the removal of patch (0, 24, and 72 hours).

Animal experiment

All studies were conducted according to ethical regulations and protocols approved by the Zhejiang University and Laboratory Animal Center. BALB/c male mice (8 to 9 weeks of age) were purchased from Hangzhou Medical College. The dorsal skin of mice (3 cm by 6 cm) was shaved and recovered for 2 days. The mice that experienced hair regrowth were excluded. From days 0 to 6, 40 mg of Vaseline cream for the control group or 40 mg of 5% imiquimod cream for the other groups was topically administrated once a day by cotton swab in a constrained area (3 cm by 2.5 cm). On day 2, 4 hours after the cream application, different groups underwent following procedures: Healthy mice (normal), no action; untreated psoriasis (untreated), adhesive tape over the naked skin; blank PMN (B-PMN)/T_{reg} cell-loaded PMN (T_{reg}-PMN)/T_{reg} cell–loaded MMN (T_{reg}-MMN), MNs (2 cm^2, 126 needles in total) applied on dorsum and fixed with adhesive tape; i.d. T_{reg}, 2×20 μl of medium of T_{reg} cells (8×10^6 cells/ml) intradermally injected on the dorsum of the mice, anesthetized with isoflurane; and i.v. T_{reg}, the medium of T_{reg} cells (1×10^7 cells/kg) systematically injected through the tail vein. The MN patches were removed 6 hours after administration. The PASI score was recorded by visual

inspection each day. On day 6, all mice were harvested for FACS, ELISA, and H&E stain analysis.

Fluorescence-activated cell sorting

FACS experiments were prepared as following: Fixable Viability Stain 510 (BD Horizon,564406), allophycocyanin-Cy7 Rat Anti-Mouse CD45 (BD Pharmingen, 30-F11,557659), fluorescein isothiocyanate (FITC) Hamster Anti-Mouse CD3e (BD Pharmingen,145-2C11,553061), BV421 Rat Anti-Mouse CD4 (BD Horizon,GK1.5,562891), Alexa Fluor 647 Rat anti-Mouse Foxp3 (BD Pharmingen, MF23,560401), peridinin-chlorophyll-protein (PerCP)–Cy5.5 Rat Anti-Mouse CD8a (BD Pharmingen,53-6.7,551162), FITC Rat Anti-CD11b (BD Pharmingen, M1/70, 557396), BV421 Hamster Anti-Mouse CD11c (BD Horizon, HL3, 562782), phycoerythrin (PE) Rat Anti-Mouse Ly-6G (BD Pharmingen, 1A8, 551461), PerCP-Cy5.5 Hamster Anti-Mouse CD3e (BD Pharmingen, 145-2C11, 551163), Alexa Fluor 647 Rat Anti-Mouse F4/80 (BD Pharmingen, T45-2342, 565853), and PE-CF594 Hamster Anti-Mouse γδT-Cell Receptor (BD Horizon, GL3,563532). All antibodies were titrated according to the guidance from manufacturer. Three skin sections (1.5 cm by 2 cm) from the same treatment group were mixed as one FACS sample to ensure sufficient cells for analysis. All flow cytometry data were processed by Beckman CytoFlex S and analyzed by FlowJo software.

Enzyme-linked immunosorbent assay

ELISA kits (MultiSciences Biotech Co. Ltd.) were conducted as the manufacturer instructed. Briefly, 100 to 200 mg of mouse dorsal skin was ground in radioimmunoprecipitation assay buffer and analyzed without dilution.

Statistical analysis

All results are presented as mean ± SD unless specified elsewhere. Statistical analysis was evaluated by GraphPad Prism7 with two-tailed Student's *t* test for group-to-group comparison and two-way analysis of variance (ANOVA) for multiple groups. The differences among groups were considered statistically significant when $^{*}P < 0.05$, $^{**}P < 0.01$, and $^{***}P < 0.001$.

Supplementary Materials

This PDF file includes:
Figs. S1 to S24
Tables S1 to S3
Legend for movie S1

Other Supplementary Material for this manuscript includes the following:
Movie S1

View/request a protocol for this paper from *Bio-protocol*.

REFERENCES AND NOTES

1. M. Dominguez-Villar, D. A. Hafler, Regulatory T cells in autoimmune disease. *Nat. Immunol.* **19**, 665–673 (2018).
2. A. Sharabi, M. G. Tsokos, Y. Ding, T. R. Malek, D. Klatzmann, G. C. Tsokos, Regulatory T cells in the treatment of disease. *Nat. Rev. Drug Discov.* **17**, 823–844 (2018).
3. J. A. Bluestone, Q. Tang, T_{reg} cells—the next frontier of cell therapy. *Science* **362**, 154–155 (2018).
4. L. Fugger, L. T. Jensen, J. Rossjohn, Challenges, progress, and prospects of developing therapies to treat autoimmune diseases. *Cell* **181**, 63–80 (2020).
5. H. Chang, S. W. T. Chew, M. Zheng, D. C. S. Lio, C. Wiraja, Y. Mei, X. Ning, M. Cui, A. Than, P. Shi, D. Wang, K. Pu, P. Chen, H. Liu, C. Xu, Cryomicroneedles for transdermal cell delivery. *Nat. Biomed. Eng.* **5**, 1008–1018 (2021).
6. K. Lee, Y. Xue, J. Lee, H. Kim, Y. Liu, P. Tebon, E. Sarikhani, W. Sun, S. Zhang, R. Haghniaz, B. Çelebi-Saltik, X. Zhou, S. Ostrovidov, S. Ahadian, N. Ashammakhi, M. R. Dokmeci, A. Khademhosseini, A patch of detachable hybrid microneedle depot for localized delivery of mesenchymal stem cells in regeneration therapy. *Adv. Funct. Mater.* **30**, 2000086 (2020).
7. C. Raffin, L. T. Vo, J. A. Bluestone, Treg cell-based therapies: Challenges and perspectives. *Nat. Rev. Immunol.* **20**, 158–172 (2020).
8. A. Rendon, K. Schäkel, Psoriasis pathogenesis and treatment. *Int. J. Mol. Sci.* **20**, 1475 (2019).
9. L. Nussbaum, Y. L. Chen, G. S. Ogg, Role of regulatory T cells in psoriasis pathogenesis and treatment. *Br. J. Dermatol.* **184**, 14–24 (2021).
10. J. E. Greb, A. M. Goldminz, J. T. Elder, M. G. Lebwohl, D. D. Gladman, J. J. Wu, N. N. Mehta, A. Y. Finlay, A. B. Gottlieb, Psoriasis. *Nat. Rev. Dis. Primers* **2**, 16082 (2016).
11. World Health Organization, *Global report on psoriasis* (World Health Organization, Geneva, 2016).
12. N. Ali, M. D. Rosenblum, Regulatory T cells in skin. *Immunology* **152**, 372–381 (2017).
13. Y. Ye, J. Yu, D. Wen, A. R. Kahkoska, Z. Gu, Polymeric microneedles for transdermal protein delivery. *Adv. Drug Deliv. Rev.* **127**, 106–118 (2018).
14. S. Zhang, J. Ermann, M. D. Succi, A. Zhou, M. J. Hamilton, B. Cao, J. R. Korzenik, J. N. Glickman, P. K. Vemula, L. H. Glimcher, G. Traverso, R. Langer, J. M. Karp, An inflammation-targeting hydrogel for local drug delivery in inflammatory bowel disease. *Sci. Transl. Med.* **7**, 300ra128 (2015).
15. B. Shashni, Y. Tajika, Y. Nagasaki, Design of enzyme-responsive short-chain fatty acid-based self-assembling drug for alleviation of type 2 diabetes mellitus. *Biomaterials* **275**, 120877 (2021).
16. Z. Liao, W. Zhang, H. Zheng, Y. Wang, J. Yu, H. Li, Z. Gu, Leveraging biomaterials for enhancing T cell immunotherapy. *J. Control Rel.* **344**, 272–288 (2022).
17. H. Wang, D. J. Mooney, Biomaterial-assisted targeted modulation of immune cells in cancer treatment. *Nat. Mater.* **17**, 761–772 (2018).
18. H. Li, Z. Wang, E. A. Ogunnaike, Q. Wu, G. Chen, Q. Hu, T. Ci, Z. Chen, J. Wang, D. Wen, H. Du, J. Jiang, J. Sun, X. Zhang, G. Dotti, Z. Gu, Scattered seeding of CAR T cells in solid tumors augments anticancer efficacy. *Natl. Sci. Rev.* **9**, nwab172 (2022).
19. L. Bao, J. Park, G. Bonfante, B. Kim, Recent advances in porous microneedles: Materials, fabrication, and transdermal applications. *Drug Deliv. Transl. Res.* **12**, 395–414 (2022).
20. H. K. Makadia, S. J. Siegel, Poly Lactic-co-Glycolic Acid (PLGA) as biodegradable controlled drug delivery carrier. *Polymers* **3**, 1377–1397 (2011).
21. S. N. Economidou, D. Douroumis, 3D printing as a transformative tool for microneedle systems: Recent advances, manufacturing considerations and market potential. *Adv. Drug Deliv. Rev.* **173**, 60–69 (2021).
22. C.-H. Chang, E. L. Pearce, Emerging concepts of T cell metabolism as a target of immunotherapy. *Nat. Immunol.* **17**, 364–368 (2016).
23. N. J. MacIver, R. D. Michalek, J. C. Rathmell, Metabolic regulation of T lymphocytes. *Annu. Rev. Immunol.* **31**, 259–283 (2013).
24. C. S. Field, F. Baixauli, R. L. Kyle, D. J. Puleston, A. M. Cameron, D. E. Sanin, K. L. Hippen, M. Loschi, G. Thangavelu, M. Corrado, J. Edwards-Hicks, K. M. Grzes, E. J. Pearce, B. R. Blazar, E. L. Pearce, Mitochondrial integrity regulated by lipid metabolism is a cell-intrinsic checkpoint for Treg suppressive function. *Cell Metab.* **31**, 422–437.e5 (2020).
25. M. D. Buck, D. O'Sullivan, R. I. Klein Geltink, J. D. Curtis, C.-H. Chang, D. E. Sanin, J. Qiu, O. Kretz, D. Braas, G. J. W. van der Windt, Q. Chen, S. C.-C. Huang, C. M. O'Neill, B. T. Edelson, E. J. Pearce, H. Sesaki, T. B. Huber, A. S. Rambold, E. L. Pearce, Mitochondrial dynamics controls T cell fate through metabolic programming. *Cell* **166**, 63–76 (2016).
26. F. Oesch, E. Fabian, K. Guth, R. Landsiedel, Xenobiotic-metabolizing enzymes in the skin of rat, mouse, pig, guinea pig, man, and in human skin models. *Arch. Toxicol.* **88**, 2135–2190 (2014).
27. N. Ohkura, Y. Kitagawa, S. Sakaguchi, Development and maintenance of regulatory T cells. *Immunity* **38**, 414–423 (2013).
28. M. Noack, P. Miossec, Th17 and regulatory T cell balance in autoimmune and inflammatory diseases. *Autoimmun. Rev.* **13**, 668–677 (2014).
29. H. Jorn Bovenschen, P. C. van de Kerkhof, P. E. van Erp, R. Woestenenk, I. Joosten, H. J. P. M. Koenen, Foxp3^{+} regulatory T cells of psoriasis patients easily differentiate into IL-17A-producing cells and are found in lesional skin. *J. Invest. Dermatol.* **131**, 1853–1860 (2011).
30. M. Rossetti, R. Spreafico, S. Saidin, C. Chua, M. Moshref, J. Y. Leong, Y. K. Tan, J. Thumboo, J. van Loosdregt, S. Albani, Ex vivo-expanded, but not in vitro-induced, human regulatory T

cells are candidates for cell therapy in autoimmune diseases due to stable demethylation of the FOXP3 TSDRa. *J. Immunol.* **194**, 113–124 (2015).
31. P. Hoffmann, T. J. Boeld, R. Eder, J. Huehn, S. Floess, G. Wieczorek, S. Olek, W. Dietmaier, R. Andreesen, M. Edinger, Loss of FOXP3 expression in natural human $CD4^+CD25^+$ regulatory T cells upon repetitive in vitro stimulation. *Eur. J. Immunol.* **39**, 1088–1097 (2009).
32. Y. Furusawa, Y. Obata, S. Fukuda, T. A. Endo, G. Nakato, D. Takahashi, Y. Nakanishi, C. Uetake, K. Kato, T. Kato, M. Takahashi, N. N. Fukuda, S. Murakami, E. Miyauchi, S. Hino, K. Atarashi, S. Onawa, Y. Fujimura, T. Lockett, J. M. Clarke, D. L. Topping, M. Tomita, S. Hori, O. Ohara, T. Morita, H. Koseki, J. Kikuchi, K. Honda, K. Hase, H. Ohno, Commensal microbe-derived butyrate induces the differentiation of colonic regulatory T cells. *Nature* **504**, 446–450 (2013).
33. P. M. Smith, M. R. Howitt, N. Panikov, M. Michaud, C. A. Gallini, M. Bohlooly-Y, J. N. Glickman, W. S. Garrett, The microbial metabolites, short-chain fatty acids, regulate colonic T_{reg} cell homeostasis. *Science* **341**, 569–573 (2013).
34. V. A. Gerriets, R. J. Kishton, M. O. Johnson, S. Cohen, P. J. Siska, A. G. Nichols, M. O. Warmoes, A. A. de Cubas, N. J. MacIver, J. W. Locasale, L. A. Turka, A. D. Wells, J. C. Rathmell, Foxp3 and Toll-like receptor signaling balance T_{reg} cell anabolic metabolism for suppression. *Nat. Immunol.* **17**, 1459–1466 (2016).
35. C. J. Voskens, D. Stoica, S. Roessner, F. Vitali, S. Zundler, M. Rosenberg, M. Wiesinger, J. Wunder, B. Siegmund, B. Schuler-Thurner, G. Schuler, C. Berking, R. Atreya, M. F. Neurath, Safety and tolerability of a single infusion of autologous ex vivo expanded regulatory T cells in adults with ulcerative colitis (ER-TREG 01): Protocol of a phase 1, open-label, fast-track dose-escalation clinical trial. *BMJ Open* **11**, e049208 (2021).
36. C. G. Brunstein, J. S. Miller, D. H. McKenna, K. L. Hippen, T. E. DeFor, D. Sumstad, J. Curtsinger, M. R. Verneris, M. L. MacMillan, B. L. Levine, J. L. Riley, C. H. June, C. Le, D. J. Weisdorf, P. B. McGlave, B. R. Blazar, J. E. Wagner, Umbilical cord blood–derived T regulatory cells to prevent GVHD: Kinetics, toxicity profile, and clinical effect. *Blood* **127**, 1044–1051 (2016).
37. L. van der Fits, S. Mourits, J. S. A. Voerman, M. Kant, L. Boon, J. D. Laman, F. Cornelissen, A.-M. Mus, E. Florencia, E. P. Prens, E. Lubberts, Imiquimod-induced psoriasis-like skin inflammation in mice is mediated via the IL-23/IL-17 Axis. *J. Immunol.* **182**, 5836–5845 (2009).
38. Y. Guo, Y.-Q. Xie, M. Gao, Y. Zhao, F. Franco, M. Wenes, I. Siddiqui, A. Bevilacqua, H. Wang, H. Yang, B. Feng, X. Xie, C. M. Sabatel, B. Tschumi, A. Chaiboonchoe, Y. Wang, W. Li, W. Xiao, W. Held, P. Romero, P.-C. Ho, L. Tang, Metabolic reprogramming of terminally exhausted $CD8^+$ T cells by IL-10 enhances anti-tumor immunity. *Nat. Immunol.* **22**, 746–756 (2021).
39. A. Naing, J. R. Infante, K. P. Papadopoulos, I. H. Chan, C. Shen, N. P. Ratti, B. Rojo, K. A. Autio, D. J. Wong, M. R. Patel, P. A. Ott, G. S. Falchook, S. Pant, A. Hung, K. L. Pekarek, V. Wu, M. Adamow, S. McCauley, J. B. Mumm, P. Wong, P. Van Vlasselaer, J. Leveque, N. M. Tannir, M. Oft, PEGylated IL-10 (Pegilodecakin) induces systemic immune activation, $CD8^+$ T cell invigoration and polyclonal T cell expansion in cancer patients. *Cancer Cell* **34**, 775–791.e3 (2018).
40. J. Baliwag, D. H. Barnes, A. Johnston, Cytokines in psoriasis. *Cytokine* **73**, 342–350 (2015).
41. H. Li, Q. Yao, A. G. Mariscal, X. Wu, J. Hülse, E. Pedersen, K. Helin, A. Waisman, C. Vinkel, S. F. Thomsen, A. Avgustinova, S. A. Benitah, P. Lovato, H. Norsgaard, M. S. Mortensen, L. Veng, B. Rozell, C. Brakebusch, Epigenetic control of IL-23 expression in keratinocytes is important for chronic skin inflammation. *Nat. Commun.* **9**, 1420 (2018).
42. Y. Cai, X. Shen, C. Ding, C. Qi, K. Li, X. Li, V. R. Jala, H. Zhang, T. Wang, J. Zheng, J. Yan, Pivotal role of dermal IL-17-producing γδ T cells in skin inflammation. *Immunity* **35**, 596–610 (2011).
43. C. Conrad, J. Di Domizio, A. Mylonas, C. Belkhodja, O. Demaria, A. A. Navarini, A.-K. Lapointe, L. E. French, M. Vernez, M. Gilliet, TNF blockade induces a dysregulated type I interferon response without autoimmunity in paradoxical psoriasis. *Nat. Commun.* **9**, 25 (2018).
44. O. Arican, M. Aral, S. Sasmaz, P. Ciragil, Serum levels of TNF-α, IFN-γ, IL-6, IL-8, IL-12, IL-17, and IL-18 in patients with active psoriasis and correlation with disease severity. *Mediators Inflamm.* **2005**, 273–279 (2005).
45. Y. Zhang, J. Yu, A. R. Kahkoska, J. Wang, J. B. Buse, Z. Gu, Advances in transdermal insulin delivery. *Adv. Drug Deliv. Rev.* **139**, 51–70 (2019).
46. L. Berod, C. Friedrich, A. Nandan, J. Freitag, S. Hagemann, K. Harmrolfs, A. Sandouk, C. Hesse, C. N. Castro, H. Bähre, S. K. Tschirner, N. Gorinski, M. Gohmert, C. T. Mayer, J. Huehn, E. Ponimaskin, W.-R. Abraham, R. Müller, M. Lochner, T. Sparwasser, De novo fatty acid synthesis controls the fate between regulatory T and T helper 17 cells. *Nat. Med.* **20**, 1327–1333 (2014).
47. R. Wang, S. Cao, M. E. H. Bashir, L. A. Hesser, Y. Su, S. M. C. Hong, A. Thompson, E. Culleen, M. Sabados, N. P. Dylla, E. Campbell, R. Bao, E. B. Nonnecke, C. L. Bevins, D. S. Wilson, J. A. Hubbell, C. R. Nagler, Treatment of peanut allergy and colitis in mice via the intestinal release of butyrate from polymeric micelles. *Nat. Biomed. Eng.* **7**, 38–55 (2023).
48. R. J. Kishton, M. Sukumar, N. P. Restifo, Metabolic regulation of T cell longevity and function in tumor immunotherapy. *Cell Metab.* **26**, 94–109 (2017).
49. A. Luengo, D. Y. Gui, M. G. Vander Heiden, Targeting metabolism for cancer therapy. *Cell Chem. Biol.* **24**, 1161–1180 (2017).
50. J. N. Clough, O. S. Omer, S. Tasker, G. M. Lord, P. M. Irving, Regulatory T-cell therapy in Crohn's disease: Challenges and advances. *Gut* **69**, 942–952 (2020).
51. J. M. Marín Morales, N. Münch, K. Peter, D. Freund, U. Oelschlägel, K. Hölig, T. Böhm, A.-C. Flach, J. Keßler, E. Bonifacio, M. Bornhäuser, A. Fuchs, Automated clinical grade expansion of regulatory T cells in a fully closed system. *Front. Immunol.* **10**, 38 (2019).
52. M. Romano, S. L. Tung, L. A. Smyth, G. Lombardi, Treg therapy in transplantation: A general overview. *Transpl. Int.* **30**, 745–753 (2017).
53. J. Han, K. Lin, C. Sequeira, C. H. Borchers, An isotope-labeled chemical derivatization method for the quantitation of short-chain fatty acids in human feces by liquid chromatography–tandem mass spectrometry. *Anal. Chim. Acta* **854**, 86–94 (2015).

Acknowledgments: We thank the technician supports at the Center of Cryo-Electron Microscopy, Zhejiang University on SEM and confocal images. **Funding:** This work was supported by the grants from the National Key R&D Program of China (2021YFA0909900) to Z.G., the National Natural Science Foundation of China (52233013) to Z.G., Zhejiang Province "Kunpeng Action" Plan to Z.G, the National Natural Science Foundation of China (32101064) to Y.Z., the Young Elite Scientists Sponsorship Program by CAST(YESS) 2022-2024QNRC001 to Y.Z., the Fundamental Research Funds for the Central Universities (2021FZZX001-47) to Y.Z., the Startup Packages of Zhejiang University to Z.G. and Y.Z., and the Zhejiang Provincial Natural Science Foundation (LY21E030007) to Y.C. **Author contributions:** Z.G., Y.Z., and W.Z. conceived the idea and designed the experiment. W.Z. designed the MN, performed the experiments, and collected the data with the help of Y.C., Z.Z., H.Z., S.W., Z.L., T.S., S.Z., W.H., and F.H. All authors discussed and analyzed the data. W.Z., H.Z., S.W., J.Y., Y.Z., and Z.G. wrote the paper. **Competing interests:** Z.G. is the cofounder of Zenomics Inc., ZenCapsule Inc., Lizen Inc., Wskin Inc., and Zcapsule Inc. Z.G. and Y.Z. are the cofounders of μZen Pharma Co. Ltd. The other authors declare that they have no competing interests. **Data and materials availability:** All data needed to evaluate the conclusions in the paper are present in the paper and/or the Supplementary Materials.

Submitted 9 January 2023
Accepted 14 April 2023
Published 17 May 2023
10.1126/sciadv.adg6007